

Time reversal symmetry breaking superconducting ground state in the doped Mott-insulator on honeycomb lattice

Zheng-Cheng Gu,¹ Hong-Chen Jiang,¹ D. N. Sheng,² Hong Yao,³ Leon Balents,¹ and Xiao-Gang Wen⁴

¹*Kavli Institute for Theoretical Physics, University of California, Santa Barbara, CA 93106, USA*

²*Department of Physics and Astronomy, California State University, Northridge, California 91330, USA*

³*Department of Physics, Stanford University, Stanford, CA 94305, USA*

⁴*Department of Physics, Massachusetts Institute of Technology, Cambridge, Massachusetts 02139, USA*

(Dated: November 29, 2021)

The emergence of superconductivity in doped Mott insulators has been debated for decades. In this paper, we report the theoretical discovery of a novel time reversal symmetry breaking superconducting ground state in the doped Mott-insulator (described by the well known t - J model) on honeycomb lattice, based on a recently developed variational method: the Grassmann tensor product state (GTPS) approach. As a benchmark, we use exact diagonalization (ED) and density matrix renormalization (DMRG) methods to check our results on small clusters. We find systematic consistency for the ground state energy as well as other physical quantities, such as the staggered magnetization. At low doping, the superconductivity coexists with anti-ferromagnetic ordering.

PACS numbers:

I. INTRODUCTION

Since the discovery of high-temperature superconductivity in cuprates¹, many strongly correlated models have been intensively studied. One of the simplest of these models is the t - J model², which describes a doped Mott-insulator:

$$H_{t-J} = t \sum_{\langle ij \rangle, \sigma} \tilde{c}_{i, \sigma}^\dagger \tilde{c}_{j, \sigma} + h.c. + J \sum_{\langle ij \rangle} \left(\mathbf{S}_i \cdot \mathbf{S}_j - \frac{1}{4} n_i n_j \right), \quad (1)$$

where $\tilde{c}_{i, \sigma}^\dagger$ is the electron operator defined in the no-double-occupancy subspace. This model can be derived from the strong-coupling limit of the Hubbard model. It is believed that such a simple model potentially captures the key mechanism of high T_c cuprates. Despite its simplicity and extensive study on it, the nature of the ground states of Eq. (1) is still controversial due to the no-double-occupancy constraint.

A strong correlation view of the t - J model was advanced by Anderson, who conjectured the relevance of a resonating valence bond (RVB) state³ as a low energy state for Eq. (1) when doped. When undoped, the RVB state is a spin singlet, with no symmetry breaking, and describes a “quantum spin liquid”. At low temperature, the mobile carriers in the doped RVB state behave as bosons and condense, forming a state indistinguishable in terms of symmetry from a singlet BCS superconductor. A further development was the introduction of a projected mean-field wavefunction – the projection removing all components of the wavefunction with doubly occupied sites – which could be used variationally^{4,5}.

Presently, this variational method remains one of the few numerical tools for t - J like models which work directly at $T = 0$ and can deal with significant system sizes. However, due to the special form of the variational wavefunction, one may be concerned about bias: very general states in the low energy subspace cannot be investigated.

Recently new numerical tools have been developed to investigate much more general low energy states in t - J like models beyond the projective method. One novel construction builds Tensor Product States (TPS's)^{7–12}, which can be conveniently studied and have been applied to many spin systems^{8–14}. This new class of variational states do not assume any specific ordering pattern a priori and can describe very general states as long as their entanglement entropies satisfy perimeter law. Recently, this method has been generalized to fermionic systems^{15–20}. Among many different generalizations, the Grassmann tensor product states (GTPS's)²⁰ were shown to be closely related to projective states. They are able to describe a class of projective wavefunctions faithfully, including the short-range RVB states in particular. Very recently, the application of this kind of new numerical method to the t - J model on square lattice has reported²¹ the discovery of a stripe state instead of the d-wave superconductivity suggested by the meanfield approach or projective wave function approach a long time ago.

Since the ground state of square lattice t - J model is still controversial, it is interesting to investigate the phase diagram of the t - J model on another lattice geometry, e.g., the honeycomb lattice. Like the square lattice appropriate for the cuprates, the honeycomb lattice is bipartite and naturally supports an antiferromagnetic (AF) state at half-filling in the strong coupling (Heisenberg) limit. Similarities to cuprate physics may be expected. Moreover, several numerical studies have identified a possible quantum spin liquid state on this lattice at half-filling when additional quantum fluctuations are included in the Hubbard⁶ and Heisenberg^{22,23} models. Thus the doped t - J model on the honeycomb lattice seems a promising venue to explore RVB ideas.

Here, we investigate the ground state of this system using the recently developed GTPS approach. The GTPS results are benchmarked by comparison with exact diagonalization (ED) and density matrix renormalization

group (DMRG) calculations. Our results are systematically consistent with these non-variational, exact methods on small clusters. The principle result of the GTPS calculations is that the ground state at non-zero doping is a time reversal symmetry breaking $d + id$ wave superconductor. Some physical rationales for this result are given at the end of this paper.

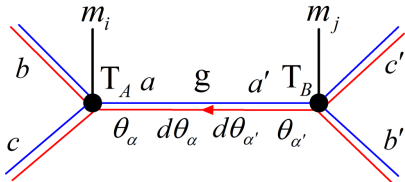


FIG. 1: (Color online) Graphic representation of the GTPS on a honeycomb lattice. \mathbf{T}_A and \mathbf{T}_B , which contain θ are defined on the sublattices A and B for each unit cell. The Grassmann metric \mathbf{g} containing $d\theta$ is defined on the links that connect the Grassmann tensors \mathbf{T}_A and \mathbf{T}_B . The blue lines represent the fermion parity even indices while the red lines represent the fermion parity odd indices of the virtual states. Notice that an arrow from A to B represents the ordering convention $d\theta_\alpha d\theta_{\alpha'}$ that we use for the Grassmann metric.

II. THE VARIATIONAL ANSATZ

We use the standard form of GTPS as our variational wavefunction. We further assume a translationally invariant ansatz, and thus it is specified by just two different Grassmann tensors $\mathbf{T}_A, \mathbf{T}_B$ on sublattice A, B of each unit cell:

$$\begin{aligned} \Psi(\{m_i\}, \{m_j\}) & \quad (2) \\ = \text{tTr} \int \prod_{\langle ij \rangle} \mathbf{g}_{aa'} \prod_{i \in A} \mathbf{T}_{A;abc}^{m_i} \prod_{j \in B} \mathbf{T}_{B;a'b'c'}^{m_j}, \end{aligned}$$

with

$$\begin{aligned} \mathbf{T}_{A;abc}^{m_i} &= T_{A;abc}^{m_i} \theta_\alpha^{P^f(a)} \theta_\beta^{P^f(b)} \theta_\gamma^{P^f(c)}, \\ \mathbf{T}_{B;a'b'c'}^{m_j} &= T_{B;a'b'c'}^{m_j} \theta_{\alpha'}^{P^f(a')} \theta_{\beta'}^{P^f(b')} \theta_{\gamma'}^{P^f(c')}, \\ \mathbf{g}_{aa'} &= \delta_{aa'} d\theta_\alpha^{P^f(a)} d\theta_{\alpha'}^{P^f(a')}. \end{aligned} \quad (3)$$

We notice that the symbol tTr means tensor contraction of the inner indices $\{a\}$. Here $\theta_{\alpha(\beta,\gamma)}, d\theta_{\alpha(\beta,\gamma)}$ are the Grassmann numbers and dual Grassmann numbers respectively defined on the link $a(b, c)$ and they satisfy the Grassmann algebra:

$$\begin{aligned} \theta_\alpha \theta_\beta &= -\theta_\beta \theta_\alpha, & d\theta_\alpha d\theta_\beta &= -d\theta_\beta d\theta_\alpha, \\ \int d\theta_\alpha \theta_\beta &= \delta_{\alpha\beta} & \int d\theta_\alpha 1 &= 0. \end{aligned} \quad (4)$$

As shown in Fig.1, $a, b, c = 1, 2, \dots, D$ are the virtual indices carrying a fermion parity $P^f(a) = 0, 1$. In this paper, we choose D to be even and assume that there are *equal* numbers of fermion parity even/odd indices, which might be not necessary in general. Those indices with odd parity are always associated with a Grassmann number on the corresponding link and the metric $\mathbf{g}_{aa'}$ is the Grassmann generalization of the canonical delta function. The complex coefficients $T_{A;abc}^{m_i}$ and $T_{B;a'b'c'}^{m_j}$ are the variational parameters.

Notice that m_i is the physical index of the t - J model on site i , which can take three different values, o, \uparrow and \downarrow , representing the hole, spin-up electron and spin-down electron states. We choose the hole representation in our calculations, and thus the hole state has an odd parity $P^f(o) = 1$ while the electron states have even parity $P^f(\uparrow, \downarrow) = 0$. On each site, the non-zero components of the Grassmann tensors should satisfy the parity conservation constraint:

$$P^f(m_i) + P^f(a) + P^f(b) + P^f(c) = 0 \pmod{2}. \quad (5)$$

Since the wavefunction Eq.(3) does not have a definite fermion number, we use the grand canonical ensemble, adding a chemical potential term to Eq.(1) to control the average hole concentration.

We use the imaginary time evolution method²⁴ to update the GTPS from a random state. Then we use the weighted Grassmann-tensor-entanglement renormalization group (wGTERG) method^{20,24} to calculate physical quantities. (See appendix sections for details.) The total system size ranges up to 2×27^2 sites and all calculations are performed with periodic boundary conditions. The largest virtual dimension of the GTPS considered is 12. To ensure convergence of the wTERG method, we keep D_{cut} (defined in Refs.^{20,24}) up to 130 for $D = 4, 6, 8, 10$, which gives relative errors for physical quantities of order 10^{-3} . For $D = 12$, we keep D_{cut} up to 152.

III. GROUND STATE ENERGY AND STAGGERED MAGNETIZATION

At half-filling, the t - J model reduces to the Heisenberg model. In this case, we find that the converged ground state energies per site are -0.5439 for $D = 10$ and -0.5441 for $D = 12$ (the term $-\frac{1}{4}n_i n_j$ is subtracted here), which are consistent with a previous TPS study¹² (with virtual dimension $D = 5$ and 6, since all the components of GTPS with odd fermion parity virtual indices vanish in this case) and a recent quantum Monte Carlo (QMC) result $E = -0.54455(20)$. Despite the good agreement with the ground state energy, the staggered magnetization $m = \sqrt{\langle S_i^x \rangle^2 + \langle S_i^y \rangle^2 + \langle S_i^z \rangle^2}$ (with $\mathbf{S}_{i \in A} = -\mathbf{S}_{i \in B}$ observed numerically) obtained from our calculations is larger than the QMC result $m = 0.2681(8)$. We find $m = 0.3257$ for $D = 10$ and $m = 0.3239$ for $D = 12$, which are also consistent with the previous TPS study¹⁰⁻¹².

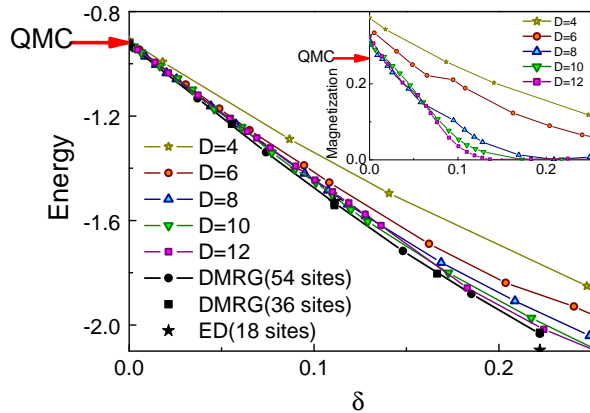


FIG. 2: (Color online) Ground state energy as a function of doping. As a benchmark, we performed the ED calculation and DMRG calculations for small system size. Inset: Stagger magnetization as a function of doping.

Nevertheless, we emphasize that the variational approach indeed does obtain the correct phase. Actually, a recent study for square lattice Heisenberg model shows that m can be consistent with the QMC result if D is sufficiently large²⁵.

Much more interesting physics arises after we dope the system. (We consider $t/J = 3$). As seen in Fig.2, the ground state energy shows a marked increase in D dependence as hole doping δ increases. As a benchmark, we perform the ED and DMRG calculations for small periodic clusters with N sites ($N = 18$ for ED and $N = 36, 54$ for DMRG). These two methods are the only unbiased methods for frustrated systems that avoid the sign problem, but they are restricted to relatively small systems. To ensure the convergence of the DMRG, we keep up to 8000 states and make the truncation errors less than 10^{-9} in our $N = 54$ calculations. Up to $D = 10$, we find a systematic convergence of the ground energy. Some data points around $\delta = 0.1$ for $D = 12$ have slightly higher energy than $D = 10$, because $D_{cut} = 152$ is still not large enough for convergence at $D = 12$.

As shown in the insert of Fig.2, the staggered magnetization m has an even larger D dependence than energy at finite doping. However, up to $D = 12$, the data appears to converge to a relatively well-defined curve indicating vanishing AF order for $\delta \gtrsim 0.1$. We also observed $\langle n_{i \in A} \rangle = \langle n_{j \in B} \rangle$ for arbitrary δ and therefore there is no commensurate charge density wave (CDW) order.

IV. SUPERCONDUCTIVITY

Next we turn to the interesting question of whether the doped antiferromagnetic Mott insulator on the honeycomb lattice supports superconductivity or not, and if so, what its pairing symmetry is. To answer this,

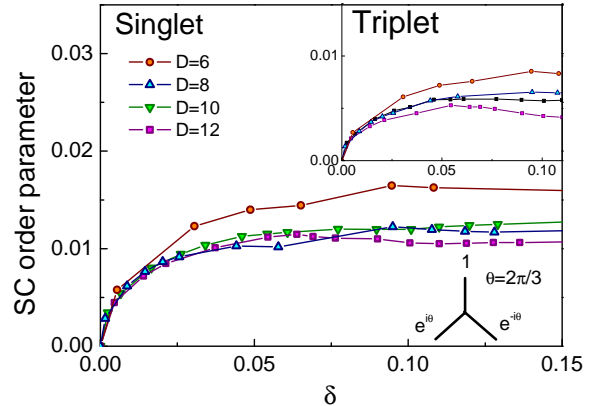


FIG. 3: SC order parameters as a function of doping.

we calculate the real space superconducting (SC) order parameters in the spin singlet channel $\Delta^s = \frac{1}{\sqrt{2}}(c_{i,\uparrow}c_{j,\downarrow} - c_{i,\downarrow}c_{j,\uparrow})$, where i and j are nearest neighbor sites. Because we use a chemical potential to control the hole concentration, the charge $U(1)$ symmetry can be spontaneously broken in the variational approach, which allows Δ^s to be measured directly rather than through its two-point correlation function. As shown in the main panel of Fig.3, up to $\delta = 0.15$ we find a non-zero singlet SC order parameter for the whole region. Strikingly, we find that the SC state breaks time reversal symmetry. By measuring the SC order parameters for the three inequivalent nearest-neighbor bonds, we found $\Delta_a^s/\Delta_b^s \simeq \Delta_b^s/\Delta_c^s \simeq \Delta_c^s/\Delta_a^s \simeq e^{i\theta}$ with $\theta = \pm \frac{2\pi}{3}$ (see Table I). This pairing symmetry is usually called $d + id$ wave. We note that the above result is quite nontrivial since we start with a completely random state without any pre-assuming SC order. Indeed, we observed that the emergence of such a $d + id$ wave SC is a consequence of gaining kinetic energy (the t term) of the t - J model during the imaginary time evolution. To exclude the possibility that this results from trapping in an unstable local minimum, we repeat the calculations with many different random tensors, and all cases converge to the same results. Moreover, we also check that the SC order parameter vanishes at large t/J to make sure that the existing SC order is the consequence of spontaneous symmetry breaking. (For $D = 6$, the critical value is around 15 at $\delta \sim 0.3$)

The existence of SC order is observed in our numerical study up to $\delta = 0.4$. However, a much larger inner dimension D is required for the convergence of ground state energy at larger hole concentration, which is beyond the scope of this paper. (The GTPS variational ansatz we use in this paper is designed to help us understand the nature of Mott physics; at large doping, the Mott physics becomes less important and can be studied much better by other methods.)

Doping	$\delta = 0.034$	$\delta = 0.101$	$\delta = 0.129$
Δ_a^s/Δ_b^s	(-0.500,-0.866)	(-0.499,-0.867)	(-0.502,-0.863)
Δ_b^s/Δ_c^s	(-0.500,-0.866)	(-0.501,-0.866)	(-0.498,-0.869)
Δ_c^s/Δ_a^s	(-0.500,-0.866)	(-0.500,-0.866)	(-0.500,-0.866)

TABLE I: Up to a very high precision, we observed $\Delta_a^s/\Delta_b^s \simeq \Delta_b^s/\Delta_c^s \simeq \Delta_c^s/\Delta_a^s \simeq e^{-\frac{2\pi i}{3}} = (-\frac{1}{2}, -\frac{\sqrt{3}}{2})$ at different hole doping for a GTPS ansatz (Here we use the data with inner dimension $D = 10$ as a simple example.)

V. COEXISTING PHASES AT LOW DOPING

Interestingly, we find the SC and AF order coexisting in the regime $0 < \delta < 0.1$. A physical consequence of the microscopic coexistence is that triplet pairing is induced. The inset of Fig.3 shows the amplitude of the triplet order parameter as a function of doping. Since the triplet pairing order parameter has three independent components $\vec{\Delta}_t = \frac{1}{\sqrt{2}}c_{i,\alpha}(i\sigma^y\vec{\sigma})_{\alpha\beta}c_{j,\beta} = \mathbf{d}e^{i\phi}$ (Here $i \in A, j \in B$ and ϕ is the phase of SC order parameter.), we can define the amplitude of triplet order parameter as $\Delta_t = \sqrt{\vec{\Delta}_t^* \cdot \vec{\Delta}_t}$. The phase shift of $2\pi/3$ on the three inequivalent bonds is also observed for all the triplet components. We further check the internal spin direction of the triplet \mathbf{d} vector and find that it is always anti-parallel to the Neel vector ($\mathbf{S}_{\text{Neel}} = \langle \mathbf{S}_i \rangle - \langle \mathbf{S}_j \rangle$). At larger doping $\delta > 0.1$, the triplet order parameter has a very strong D dependence, so at present we are unable to determine whether it ultimately vanishes or remains non-zero in the $D \rightarrow \infty$ limit. We leave this issue for future work. By fully using all symmetry quantum numbers and other techniques like high performance simulation on GPUs, we can in principle deal with D up to 20 – 30.

VI. DISCUSSIONS

The variational ansatz in this paper ignores any possible incommensurate phases. Natural candidates are spiral or striped anti-ferromagnetic phases, as having been intensively discussed for the square lattice. A weak coupling perspective suggests that this may be unlikely.

In the weak-coupling limit of the Hubbard model on honeycomb lattice, the system is a semimetal with two Dirac cones. With a non-zero Hubbard U , commensurate AF fluctuations at zero momentum manifest in the inter-band susceptibility, becoming stronger and stronger with increasing U . At sufficiently large U commensurate AF order develops (recent numerics find a narrow region of intermediate spin liquid phase⁶). At small but finite doping, the Dirac cones become pockets. In this case, the total intra-band spin susceptibility shows a constant behavior for small q ($q < 2k_f$)²⁶ while the total inter-band spin susceptibility still has a peak at zero momentum. Thus, we argue that the commensurate AF fluctuations at zero momentum still dominate for sufficiently small

hole concentration.

Our DMRG calculations also support this argument. Up to 54 sites, we do not find any evidence for incommensurate spin-spin correlation. As seen in Figs. 4(a) and 4(b), we plot the spin structure factors for the same sublattice and for different sublattices:

$$S_{AA}(\mathbf{k}) = \frac{1}{N} \sum_{i \in A; j \in A} e^{i\mathbf{k} \cdot (\mathbf{r}_i - \mathbf{r}_j)} \langle \mathbf{S}_i \cdot \mathbf{S}_j \rangle$$

$$S_{AB}(\mathbf{k}) = \frac{1}{N} \sum_{i \in A; j \in B} e^{i\mathbf{k} \cdot (\mathbf{r}_i - \mathbf{r}_j)} \langle \mathbf{S}_i \cdot \mathbf{S}_j \rangle, \quad (6)$$

where N is the total number of unit cells, which is $18(6 \times 3)$ in our DMRG calculation. We find that both S_{AA} and S_{AB} have peaks at $\mathbf{k} = (0, 0)$, with a positive value and a negative value. Such a result implies a ferromagnetic long range order for the same sublattice but a anti-ferromagnetic long range order for different sublattices. Although the system size in our DMRG calculation may be not large enough, we believe the conclusion is still correct in the thermodynamic limit since other calculation, e.g., meanfield theory, also supports this result. On the other hand, as we know that superconductivity is incommensurate with incommensurate magnetic orders, any magnetic order that coexists with superconductivity must be commensurate.

On the other hand, we find that the GTPS results are comparable with extrapolations of (commensurate)staggered magnetization m for infinite size systems (the GTPS results for m are somewhat larger when close to half-filling due to insufficient tensor dimension D). Fig. 5 shows the comparison of DMRG calculations and GTPS calculations for staggered magnetization m in small systems.

A more general concern is whether the GTPS tends to overestimate SC order at large doping, due to its non-conservation of charge (note that the projected wavefunction approach has a rather strong tendency to produce superconducting states). The observed SC order parameter is “small” in terms of the natural upper limit $\langle cc \rangle \lesssim 0.1\delta \ll \delta$. Nevertheless, our prediction of $d + id$ pairing symmetry is supported by other approaches: (a) in the mean field theory for the honeycomb t - J model, only the $d + id$ pairing channel gains energy^{27,28}, therefore $d + id$ pairing symmetry is most possible if the ground state of t - J model is a superconductor and (b) in the weak coupling limit of the Hubbard model, very recent renormalization group studies also find $d + id$ superconductivity around quarter filling^{29–33}. However, we believe that the mechanism of superconductivity discovered at low doping is a consequence of strong interaction and is quite different from the weak coupling case. Apparently our results can not be explained by any weak coupling theory, as the Dirac cone is stable at low doping (e.g., $\delta < 0.1$) and there is no superconductivity. The recently proposed skyrmion superconductivity is a very promising candidate³⁴ and we will explore this kind of idea in our future work.

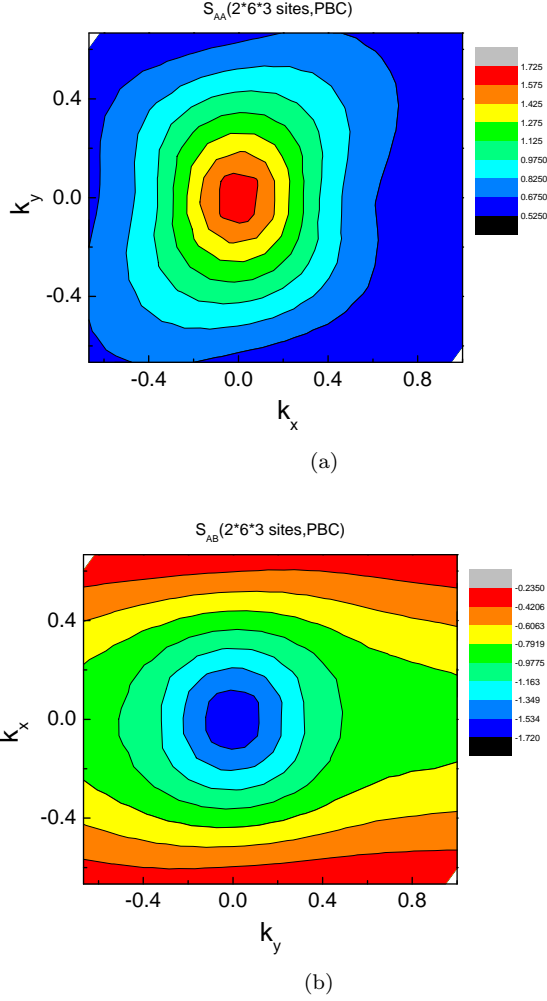


FIG. 4: (Color online) Counter plots for the spin structure factors for the same sublattice and for different sublattices. We obtain the results by performing high precision DMRG algorithm on a small cluster($2 * 6 * 3$ sites) at 5.5% doping with periodic boundary condition(PBC).

In conclusion, we report the theoretical discovery of a $d + id$ wave superconducting ground state in the t - J model on a honeycomb lattice, based on a recently developed variational method - the GTPS approach. At low doping, AF order coexists with the SC order. In the coexistence regime, a spin triplet pairing with the same phase shift is induced and its triplet \mathbf{d} vector is antiparallel with the Neel vector. It would be interesting to search for this physics in experiment. The recently discovered spin 1/2 honeycomb lattice antiferromagnet $\text{InV}_{1/3}\text{Cu}_{2/3}\text{O}_3$ ³⁵ would be an appealing candidate if it could be doped experimentally.

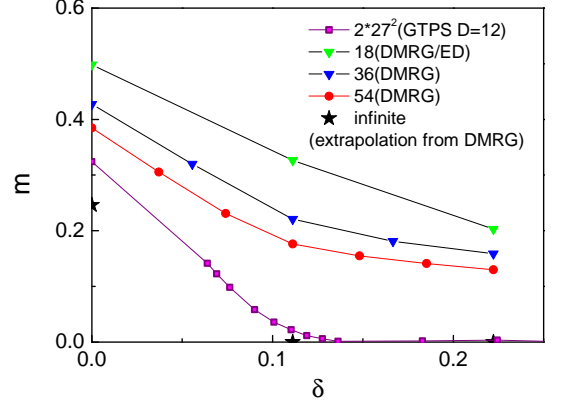


FIG. 5: (Color online)The comparison of DMRG/ED and GTPS calculations for stagger magnetization m .

Acknowledgment

The authors would like to thank F. Verstraete, J. I. Cirac, M. P. A. Fisher, F. C. Zhang, P. A. Lee, Z. Y. Weng, L. Fu, K. Sun, C. Wu, F. Yang and Y. Zhou for valuable discussions. Z.C.G. is supported by NSF Grant No. PHY05-51164; H.C.J was supported in part by the National Basic Research Program of China Grant 2011CBA00300, 2011CBA00302; D.N.S is supported by DMR-1205734 and DMR-0906816 ; L.B. is supported by NSF grant DMR-0804564 and a Packard Fellowship; H.Y. was partly supported by DOE grant DE-AC02-05CH11231; X.G.W. is supported by NSF Grant No. DMR-1005541 and NSFC 11074140.

Appendix A: The imaginary time evolution algorithm of GTPS

In this paper, we use the (simplified) imaginary time evolution method²⁴ to update the GTPS variational wave function. In the hole representation, we can decompose the $\tilde{c}_{i,\sigma}^\dagger$ as $\tilde{c}_{i,\sigma} = h_i^\dagger b_{i,\sigma}$. Here the holon h_i is a fermion while the spinon $b_{i,\sigma}$ is a boson. The no-double-occupancy constraint reads:

$$\sum_{\sigma} b_{i,\sigma}^\dagger b_{i,\sigma} + h_i^\dagger h_i = 1 \quad (\text{A1})$$

Under this representation, we can rewrite the t - J model as:

$$H_{t-J} = -t \sum_{\langle ij \rangle, \sigma} h_j^\dagger h_i b_{i,\sigma}^\dagger b_{j,\sigma} + h.c. + J \sum_{\langle ij \rangle} \left(\mathbf{S}_i \mathbf{S}_j - \frac{1}{4} n_i^b n_j^b \right), \quad (\text{A2})$$

where

$$\mathbf{S}_i = \sum_{\sigma\sigma'} b_{i,\sigma}^\dagger \boldsymbol{\tau}_{\sigma\sigma'} b_{i,\sigma'}; \quad n_i^b = \sum_{\sigma} b_{i,\sigma}^\dagger b_{i,\sigma} \quad (\text{A3})$$

Due to the no-double-occupancy constraint Eq. (A1), the spin up/down states $|\uparrow(\downarrow)_i\rangle = b_{i;\uparrow(\downarrow)}^\dagger|0\rangle$ and the hole state $|o\rangle = h_i^\dagger|0\rangle$ form a complete basis for each site. The closure condition reads:

$$|\uparrow_i\rangle\langle\uparrow_i| + |\downarrow_i\rangle\langle\downarrow_i| + |o_i\rangle\langle o_i| = 1 \quad (\text{A4})$$

As already has been discussed in Ref.²⁴, we need to use the fermion coherent state representation to perform the imaginary time evolution algorithm for GTPS. Let us introduce the fermion coherent state of holon $|\eta_i\rangle = |0\rangle - \eta_i h_i^\dagger|0\rangle$. (η_i is a Grassmann variable here.) In this new basis, the closure relation Eq. (A5) becomes:

$$|\uparrow_i\rangle\langle\uparrow_i| + |\downarrow_i\rangle\langle\downarrow_i| + \int d\bar{\eta}_i d\eta_i |\eta_i\rangle\langle\bar{\eta}_i| = 1 \quad (\text{A5})$$

The variational ground state can be determined through imaginary time evolution:

$$|\Psi_G\rangle = e^{-\tau H_{t-J}}|\Psi_0\rangle, \quad \tau \rightarrow \infty \quad (\text{A6})$$

For a sufficiently thin time slice $\delta\tau$, we can decompose $e^{-\delta\tau H_{t-J}}$ as:

$$e^{-\delta\tau H_{t-J}} \sim e^{-\delta\tau H_{t-J}^x} e^{-\delta\tau H_{t-J}^y} e^{-\delta\tau H_{t-J}^z} \quad (\text{A7})$$

Here x, y, z represent three different directions of the honeycomb lattice and each $H_{t-J}^{x(y,z)}$ term contains a summation of non-overlapped two body Hamiltonian $H_{t-J}^{x(y,z)} = \sum_{\langle ij\rangle} h_{ij}^{x(y,z)}$. Thus, for a sufficiently thin time slice, we can apply the evolution operator along the $x(y, z)$ direction separately.

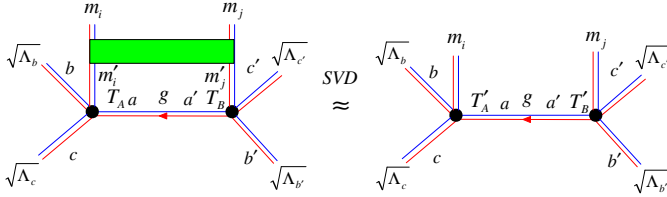


FIG. 6: (Color online) A schematic plot for the imaginary time evolution algorithm.

By applying the method developed in Ref.²⁴, we can successfully update the (complex) variational parameters $T_{A;abc}^{m_i}$ and $T_{B;a'b'c'}^{m_j}$ as:

$$T_{A;abc}^{m_i} = (-)^{P^f(m_i)P^f(a)} \frac{\sqrt{\Lambda'_a}}{\sqrt{\Lambda_b^y \Lambda_c^z}} U_{bcm_i;a}$$

$$T_{B;a'b'c'}^{m_j} = (-)^{P^f(m_j)P^f(a')} \frac{\sqrt{\Lambda'_{a'}}}{\sqrt{\Lambda_b^y \Lambda_c^z}} V_{b'c'm_j;a'}, \quad (\text{A8})$$

where U and V are determined by the singular value

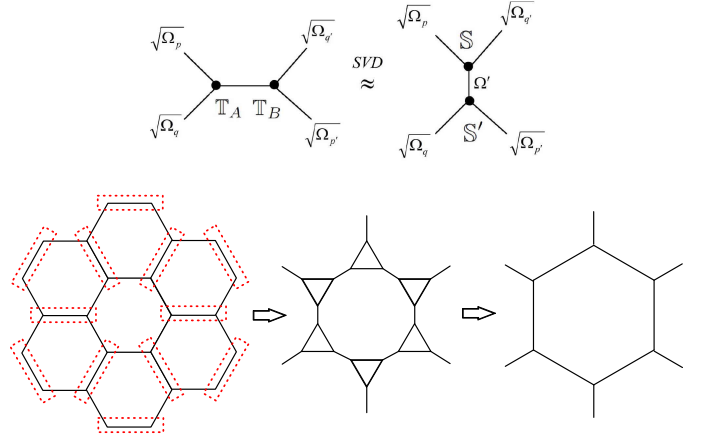


FIG. 7: (Color online) A schematic plot for the renormalization algorithm on honeycomb lattice. Similar to the simplified imaginary time evolution algorithm, we use a weighting vector $\sqrt{\Omega}$ to mimic the environment effect. As has been discussed in Ref.²⁴, the initial value of Ω can be determined by Λ on the corresponding link and will be updated during the RG scheme.

decomposition(SVD) of the following matrix M :

$$M_{bcm_i;b'c'm_j} = \sum_{am'_im'_j} \sqrt{\Lambda_b^y} \sqrt{\Lambda_c^z} \sqrt{\Lambda_{b'}^y} \sqrt{\Lambda_{c'}^z}$$

$$\times (-)^{[P^f(m'_i)+P^f(m'_j)]P^f(a)} (-)^{P^f(m'_j)[P^f(m'_i)+P^f(b)+P^f(c)]}$$

$$\times (-)^{m_j[P^f(m_i)+P^f(b)+P^f(c)]} E_{m'_im'_j}^{m_im_j} T_{A;abc}^{m'_i} T_{B;a'b'c'}^{m'_j} \quad (\text{A9})$$

Here $E_{m'_im'_j}^{m_im_j}$ is the matrix elements of the evolution operator $e^{-\delta h_{ij}^x}$ under the Fock basis. We keep the largest D th singular values:

$$M_{bcm_i;b'c'm_j} \simeq \sum_{a=1}^D U_{bcm_i;a} \Lambda'_a V_{b'c'm_j;a} \quad (\text{A10})$$

Similar to the usual TPS case¹⁰, the environment weight vectors $\Lambda^{x(y,z)}$ can be initialized as 1 and then updated during the time evolution. For example, Λ^x is updated as Λ' in the above evolution scheme.

Appendix B: The GTERG/wGTERG algorithm

After determining the variational ground state of GTPS by performing the imaginary time evolution, we can compute the physical quantities by using the GTERG/wGTERG method developed in Refs^{20,24}. This method can be regarded as the Grassmann variable generalization of the usual TERG/wTERG method^{9,24}, where a coarse graining procedure is designed to calculate the physical quantities of TPS efficiently. In Fig.8, we plot the variational ground state energy ($D = 10$) as a

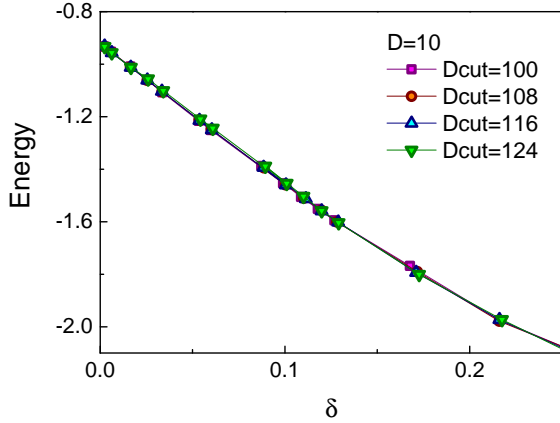


FIG. 8: (Color online) Variational ground state energy ($D = 10$) as a function of doping with different D_{cut} (Number of eigenvalues kept in the wGTERG algorithm). It is shown that all the data points almost collapse on the same curve. We find that the relative error is of order 10^{-3} .

function of doping with different D_{cut} (Number of eigenvalues kept in the wGTERG algorithm). We find that the relative error is of order 10^{-3} .

-
- ¹ J. G. Bednorz and K. A. Mueller, *Z. Phys. B* **64**, 189 (1986).
- ² F. C. Zhang and T. M. Rice, *Phys. Rev. B* **37**, 3759 (1988).
- ³ P. W. Anderson *Science* **235**, 1196 (1987).
- ⁴ C. Gros *Phys. Rev. B* **38**, 931 (1988).
- ⁵ For a review, see P. A. Lee, N. Nagaosa and X. G. Wen, *Phys. Mod. Phys.* **78**, 17 (2006).
- ⁶ Z. Y. Meng, T. C. Lang, S. Wessel, F. F. Assaad and A. Muramatsu, *Nature* **464**, 847 (2010).
- ⁷ F. Verstraete and J. I. Cirac, (2004), arXiv:cond-mat/0407066.
- ⁸ J. Jordan, R. Orus, G. Vidal, F. Verstraete, and J. I. Cirac, *Physical Review Letters* **101**, 250602 (2008).
- ⁹ Z.-C. Gu, M. Levin, and X.-G. Wen, *Phys. Rev. B* **78**, 205116 (2008).
- ¹⁰ H. C. Jiang, Z. Y. Weng, and T. Xiang, *Phys. Rev. Lett.* **101**, 090603 (2008);
- ¹¹ Z. Y. Xie, H. C. Jiang, Q. N. Chen, Z. Y. Weng, and T. Xiang, *Phys. Rev. Lett.* **103**, 160601 (2009);
- ¹² H. H. Zhao, Z. Y. Xie, Q. N. Chen, Z. C. Wei, J. W. Cai, and T. Xiang, *Phys. Rev. B* **81**, 174411 (2010).
- ¹³ B. Bauer, G. Vidal, and M. Troyer, *J.Stat.Mech.* (2009). p09006.
- ¹⁴ V. Murg, F. Verstraete, and J. I. Cirac, *Phys. Rev. B* **79**, 195119 (2009).
- ¹⁵ C. V. Kraus, N. Schuch, F. Verstraete, and J. I. Cirac *Phys. Rev. A* **81**, 052338 (2010).
- ¹⁶ P. Corboz, R. Orus, B. Bauer, and G. Vidal, *Phys. Rev. B* **81**, 165104 (2010).
- ¹⁷ T. Barthel, C. Pineda, and J. Eisert, *Phys. Rev. A* **80**, 042333 (2009).
- ¹⁸ Q. Q. Shi, S. H. Li, J. H. Zhao, and H. Q. Zhou, (2009), arXiv:cond-mat/0907.5520.
- ¹⁹ Iztok Pizorn, and Frank Verstraete, *Phys. Rev. B* **81**, 245110 (2010).
- ²⁰ Z.-C. Gu, F. Verstraete, and X.-G. Wen, (2010), arXiv:cond-mat/1004.2563.
- ²¹ P. Corboz, S. R. White, G. Vidal, and M. Troyer, *Phys. Rev. B* **84**, 041108 (2011).
- ²² J. B. Fouet, P. Sindzingre, and C. Lhuillier, *Eur. Phys. J. B* **20**, 241 (2001).
- ²³ B. K. Clark, D. A. Abanin, and S. L. Sondhi, *Phys. Rev. Lett.* **107**, 087204 (2011);
- ²⁴ Z.-C. Gu, *Phys. Rev. B* **88**, 115139 (2013).
- ²⁵ Ling Wang, Iztok Pizorn, and Frank Verstraete, *Phys. Rev. B* **83**, 134421 (2011).
- ²⁶ E. H. Hwang, and S. Das Sarma, *Phys. Rev. B* **75**, 205418 (2007).
- ²⁷ A. M. Black-Schaffer, and S. Doniach, *Phys. Rev. B* **75**, 134512 (2007).
- ²⁸ S. Pathak, V. Shenoy, and G. Baskaran, *Phys. Rev. B* **81**, 085431 (2010).
- ²⁹ K. Kuroki, *Phys. Rev. B* **81**, 104502 (2010).
- ³⁰ S. Raghu, and S. A. Kivelson, *Phys. Rev. B* **83**, 094518 (2010).
- ³¹ R. Nandkishore, L. Levitov, and A. Chubukov, *Nature Physics* **8**, 158 (2012).
- ³² W.-S. Wang, Y.-Y. Xiang, Q.-H. Wang, F. Wang, F. Yang, and D. H. Lee, *Phys. Rev. B* **85**, 035414 (2012).
- ³³ M. Kiesel, C. Platt, W. Kanke, D. A. Abanin, and R. Thomale, *Phys. Rev. B* **86**, 020507 (2012).
- ³⁴ G. Baskaran, (2011), arXiv:cond-mat/1108.3562.
- ³⁵ A. Möller, U. Löw, T. Taetz, M. Kriener, G. André, F. Damay, M. Braden, and J. A. Mydosh, *Phys. Rev. B* **78**, 024420 (2008).